Earth and Planetary Science Letters 317-318 (2012) 196–203

Contents lists available at SciVerse ScienceDirect

Earth and Planetary Science Letters

journal homepage: www.elsevier.com/locate/epsl

Rupture speed and slip velocity: What can we learn from simulated earthquakes?

Andrea Bizzarri *

Istituto Nazionale di Geofisica e Vulcanologia, Sezione di Bologna, Italy

ARTICLE INFO

Article history:
Received 20 June 2011
Received in revised form 3 November 2011
Accepted 19 November 2011
Available online 27 December 2011

Editor:L. Stixrude

Keywords:
seismic source
rupture velocity
computational sesimology
rheology of fault zones

ABSTRACT

In this paper we consider a wide catalog of synthetic earthquakes, numerically modeled as spontaneous, fully dynamic, 3-D ruptures on extended faults, governed by different friction laws, including slip-dependent and rate- and state-dependent equations. We analyze the spatial correlations between the peak of fault slip velocity (v_{peak}) and the rupture speed (v_r) at which the earthquake spreads over the fault. We found that v_{peak} positively correlates with v_r and that the increase of v_{peak} is roughly quadratic. We found that near the transition between sub- and supershear regimes v_{peak} significantly diminishes and then starts to increase again with the square of v_r. This holds for all the governing models we consider and for both homogeneous and heterogeneous configurations. Moreover, we found that, on average, v_{peak} increases with the magnitude of the event ($v_{peak} \sim M_0^{0.18}$). Our results can be incorporated as constraints in the inverse modeling of faults.

1. Introduction

Understanding the physical and chemical dissipative processes taking place during an earthquake is of pivotal importance in the mechanics of faulting. Fully dynamic models of spontaneously spreading ruptures give us the extraordinary chance to investigate the features of the constitutive law assumed to govern the fault surface, under conditions that are very often far of being properly reproduced in laboratory experiments.

One of the goals of modern-days seismology is to design robust and computationally efficient numerical codes able to generate a catalog of synthetic events and to simulate the synthetic motions recorded on the ground (i.e., on the free surface). The physics-based earthquake (forward) source models appear to be crucial for realistic ground motion simulation and seismic hazard analysis; when seismological data are rare (or even non-existent), numerical experiments can be used in order to predict ground motions caused by future earthquakes. At the same time, it is not obvious what is the most appropriated governing model to describe the breakdown mechanism occurring during slip failures (see Bizzarri, 2011b and references cited therein for a discussion).

Investigations of possible spatial correlations between the various dynamic variables, such as fracture energy density, stress drop, total developed slip, peak fault slip velocity (v_{peak}) and rupture speed (v_r) are important because they could be inserted as constraints in kinematic modeling of faults, on which current practice in seismic engineering relies.

By performing laboratory experiments of a mode II crack expanding in a granite sample, the following direct dependence between v_{peak} and v_r has been proposed (Ohnaka et al., 1987):

$$v_{peak} \cong v_r \frac{\Delta\tau_b}{G} \tag{1}$$

where $\Delta\tau_b$ is the breakdown stress drop (expressing the difference between the upper and residual stress levels) and G is the rigidity of the elastic medium. Notably, in laboratory only fracture on intact rocks experiments give the rupture speed, contrarily to friction experiments, both rotary shear and sandwich-like, where two pre-existing surfaces slide against each other (and thus without the existence of a crack tip).

In their pseudodynamic earthquake source modeling Guatteri et al. (2004) try to understand the spatial interdependency of the earthquake source parameters, such as v_r and the total slip (u_{tot}). Schmedes et al. (2010a) analyze a series of dynamic models obeying the linear slip-weakening friction to find correlations between various source parameters. On the other hand, Song et al. (2009) explore the spatial coherence between u_{tot} and v_r, and between u_{tot} and v_{peak} by analyzing kinematic rupture models of two large strike–slip events (this analysis has been then extended to dynamic models by Song and Sommerville, 2010). Bizzarri (2010c) thoroughly discusses the relations between the fracture energy and different physical observables, such as v_r, u_{tot} and the dynamic stress drop, by analyzing spontaneous dynamic earthquake models obeying different governing models.

Given the above-mentioned results, with this study we aim to understand whether, and how, v_{peak} and v_r correlate. Both of these two source parameters have a fundamental role in ground motion

* Via Donato Creti, 12, 40128 Bologna, Italy. Tel.: +39 051 4151432; fax: +39 051 4151499.
E-mail address: bizzarri@bo.ingv.it.

0012-821X/$ – see front matter © 2011 Elsevier B.V. All rights reserved.
doi:10.1016/j.epsl.2011.11.023

prediction and hazard assessment, in that the fault slip velocity is linearly related to the ground velocity (through the representation theorem; Aki and Richards, 2002) and the rupture speed controls the frequency content of the recorded particle velocity (Bizzarri et al., 2010). Moreover, v_{peak} (and its time occurrence) has received much attention because it has been proposed as a way to infer the characteristic distance over which the stress release is accomplished (Mikumo et al., 2003; see also Tinti et al., 2004).

2. Methodology

In this paper we consider synthetic earthquakes that represent the solution of the fundamental elastodynamic equation for planar faults, where 3-D spontaneous (i.e., without prior imposed v_r) rupture expand bilaterally, starting from an imposed hypocenter. The solution is obtained numerically (Bizzarri and Cocco, 2005), while the nucleation procedure is the same as in previous papers (Bizzarri, 2009, 2010c).

We consider a large number of governing models, including the linear–slip weakening (SW henceforth) function, the rate- and state-dependent (RS) friction laws, the flash heating (FH) law and a version of RS laws (referred to as CH law), where an explicit dependence on the temperature T^f developed by frictional heat is incorporated (Chester and Higgs, 1992). All the equations are recalled in Table 1; readers can refer to Bizzarri (2011b) for a thorough review of these constitutive models. We also consider a set of simulations where a viscous rheology is assumed when melting is occurring, following the physical model recently proposed (Bizzarri, 2011a). In this case the elastic parameters are different with respect to those listed in Table 2; we have $v_S = 3.464$ km/s and $v_P = 6$ km/s. Finally, we report results pertaining to fault structures where the lubrication process is active (Bizzarri, submitted for publication); this is formally a non linear SW law, which can be in some sense physically associated to the melting rheology.

Both homogeneous and heterogeneous conditions are considered in the present study; the former have all the parameters spatially identical over the whole fault, while the latter are characterized by a heterogeneous initial shear stress having a magnitude τ_0 which follows a k^{-1} behavior at high radial wavenumbers k, which corresponds in the static limit to the "k–square" model of slip at high wavenumbers. This approach, which namely follows equation (21) in Bizzarri (2010c), is very similar to that recently proposed by Andrews and Barral (2011).

Table 2
Reference parameters adopted in the present paper.

Parameter	Value
Medium and discretization parameters	
Lamé constants, $\lambda = G$	27 GPa
S wave velocity, v_S	3 km/s
P wave velocity, v_P	5.196 km/s
Cubic mass density, ρ	3000 kg/m^3
Fault length, L^f	2×6 km[a]
Fault width, W^f	11.6 km
Spatial grid size, Δx	8 m [(b)]
Time step, Δt	4.44×10^{-4} s[b]
Coordinates of the hypocenter, H $\equiv (\xi_1^H, \xi_3^H)$	(5.992,7)km
Fault constitutive parameters	
Effective normal stress, σ_n^{eff}	120 MPa
a) Slip-weakening law	
Magnitude of the initial shear stress, τ_0	70.52 MPa
Static level of friction coefficient, μ_u	0.73167 ($\leftrightarrow \tau_u = 87.80$ MPa)
Kinetic level of friction coefficient, μ_f	0.54333 ($\leftrightarrow \tau_f = 65.20$ MPa)
Characteristic slip-weakening distance, d_0	0.05 m
b) Ruina–Dieterich law	
Logarithmic direct effect parameter, a	0.016
Evolution effect parameter, b	0.020
Scale length for state variable evolution, L	0.02 m
Reference value of friction coefficient at low slip rates, μ_*	0.56
Initial sliding velocity, v_0	1×10^{-4} m/s
Magnitude of the initial shear stress, τ_0	70.52 MPa
c) Flash heating law	
Reference value of friction coefficient at high slip rates, μ_{fh}	0.13
Initial sliding velocity, v_0	1×10^{-4} m/s
Magnitude of the initial shear stress, τ_0	70.52
d) Chester–Higgs law	
Reference temperature, $T_* = T^f(t=0)$	483.15 K
Activation energies, Q_a and Q_b	1×10^5 J/mol
Universal gas constant, R	8.314472 J/(K mol)

[a] The rupture expands bilaterally starting from the hypocenter.
[b] For the adopted parameters the Courant–Friedrichs–Lewy ratio, $\omega_{CFL} = {}_{\rm df} v_S \Delta t/\Delta x$, equals 0.1665 and the estimate of the critical frequency for spatial grid dispersion, $f_{acc}^{(s)} = v_S/(6\Delta x)$, equals 62.5 Hz.

Table 1
Analytical equations for the considered governing models which give the value of the traction τ in a generic fault point $\boldsymbol{\xi}$ and at time t. Readers can refer to Bizzarri (2011b) for a thorough discussion, a description of the different quantities and for a complete list of references.

Constitutive model	Equations	Reference equation in Bizzarri (2011b)
Linear slip-weakening law (SW)	$\tau = \begin{cases} \left[\mu_u - (\mu_u-\mu_f)\dfrac{u}{d_0}\right]\sigma_n^{eff} & ,u<d_0 \\ \mu_f \sigma_n^{eff} & ,u\geq d_0 \end{cases}$	(25)
Ruina–Dieterich law (RD)	$\begin{cases} \tau = \left[\mu_* + a\ln\left(\dfrac{v}{v_*}\right) + \Theta\right]\sigma_n^{eff} \\ \dfrac{\mathrm{d}}{\mathrm{d}t}\Theta = -\dfrac{v}{L}\left[\Theta + b\ln\left(\dfrac{v}{v_*}\right)\right] \end{cases}$	(35)
Dieterich–Ruina law (RD)	$\begin{cases} \tau = \left[\mu_* + a\ln\left(\dfrac{v}{v_*}\right) + b\ln\left(\dfrac{\Psi v_*}{L}\right)\right]\sigma_n^{eff} \\ \dfrac{\mathrm{d}}{\mathrm{d}t}\Psi = 1 - \dfrac{\Psi v}{L} \end{cases}$	(33)
Chester–Higgs law (CH)	$\begin{cases} \tau = \left[\mu_* + a\ln\left(\dfrac{v}{v_*}\right) + \Theta + \dfrac{a\,Q_a}{R}\left(\dfrac{1}{T^f} - \dfrac{1}{T_*}\right)\right]\sigma_n^{eff} \\ \dfrac{\mathrm{d}}{\mathrm{d}t}\Theta = -\dfrac{v}{L}\left[\Theta + b\ln\left(\dfrac{v}{v_*}\right) + \dfrac{bQ_b}{R}\left(\dfrac{1}{T^f} - \dfrac{1}{T_*}\right)\right] \end{cases}$	(48)
Flash heating law (FH)	$\begin{cases} \tau = \left[\mu_* + a\ln\left(\dfrac{v}{v_*}\right) + \Theta\right]\sigma_n^{eff} \\ \dfrac{\mathrm{d}}{\mathrm{d}t}\Theta = -\dfrac{v}{L}\left[\Theta + b\dfrac{v_{fh}}{v}\ln\left(\dfrac{v}{v_*}\right) + \left(1 - \dfrac{v_{fh}}{v}\right)\left(a\ln\left(\dfrac{v}{v_*}\right) + \mu_* - \mu_{fh}\right)\right] \end{cases}$	(46)
Time-weakening law (TW)	$\tau = \begin{cases} \left[\mu_u - (\mu_u-\mu_f)\dfrac{(t-t_r)}{t_0}\right]\sigma_n^{eff} & ,t-t_r<t_0 \\ \mu_f \sigma_n^{eff} & ,t-t_r\geq t_0 \end{cases} \quad t_r = \dfrac{\lVert \boldsymbol{\xi} - \boldsymbol{\xi}^H \rVert}{v_r}$	(23)

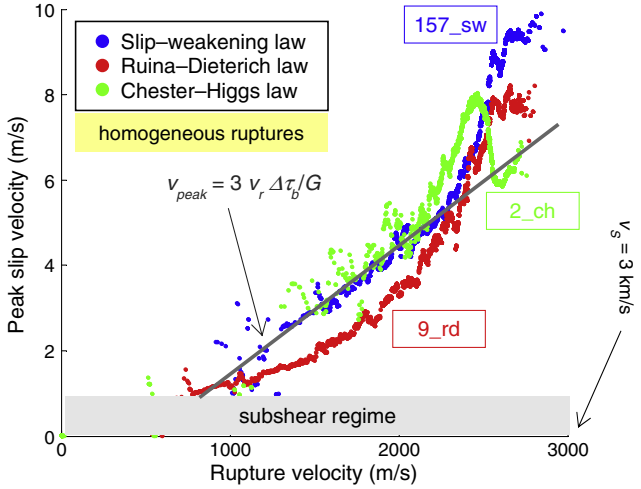

Fig. 1. Behavior of the peak slip velocity v_{peak} as a function of the rupture velocity v_r for different governing models (the equations are reported in Table 1) in the case of subshear earthquakes; for the CH law the temperature evolution is computed as described in Bizzarri (2010b). For comparison we plot as solid gray line the theoretical prediction of $v_{peak} \propto v_r$ (see Eq. (1)). Table 2 lists the adopted parameters.

In the remainder of the paper we will consider as v_{peak} the absolute maximum of the fault slip velocity time series, while v_r is computed as the inverse of the slowness (see equation (12) of Bizzarri and Spudich, 2008). Both of these two quantities are local dynamic variables, in that they are defined at each fault node.

3. Numerical results

We report in Fig. 1 the comparison between the results pertaining to three different friction models, the SW law, the Ruina–Dieterich (RD) law and the CH law. Both of these representative models have the same initial conditions and are energetically comparable, in that they have the same fracture energy density, and are characterized by governing parameters guaranteeing a subshear rupture propagation (see Table 2). The resulting behavior is very similar in all the cases; it is clear that v_{peak} does not increase linearly with v_r, as predicted by the theoretical relation (1), but a quadratic increase of peak slip velocity with the rupture speed emerges. For comparison, we superimpose in Fig. 1 a linear relation $v_{peak} \propto v_r$ (solid gray line) to emphasize the general disagreement with Eq. (1). The evolution of v as a function of the strike coordinate and at the hypocentral depth for the RD case in Fig. 1 is reported in Fig. 3b of Bizzarri (2010c).

Further complications arise when a supershear rupture propagation regime is considered, where the ruptures eventually reach the compressional wave speed (as theoretically first demonstrated by Burridge, 1973, for cohesionless cracks). In the configurations reported in Fig. 2a the parameters of the SW and RD laws and the inclusion of the flash heating of the asperity contacts allow for a sustained supershear dynamic propagation. We remark that flash heating is known to produce very high values of v_{peak}, even in 3-D (Bizzarri, 2009) and that the SW simulation presented in Fig. 2a is very unstable (the strength parameter is 0.13) and thus it produces huge values of v_{peak}. It should be also noted that, in general, once the transition to supershear regime is realized, the rupture is energetically favored (Bhat et al., 2007; Freund, 1979). We can appreciate, for all the models, an abrupt drop of v_{peak} in corresponding to the transition from sub- to supershear regimes; slightly after the S wave speed v_S, v_{peak} significantly decreases and then it continues to increase again in the supershear regime. The same holds also in the case when melting or rocks is considered (see Fig. 2b), as in Bizzarri (2011a). Also in this case, due to the dramatic stress drop experienced by the fault, the rupture is very unstable and also in this case significant values of v_{peak} are attained locally.

Fig. 3 reports the comparison of two heterogeneous configurations, where the parameters are the same as in Fig. 1 for both SW and RD laws, but now the initial shear stress has a k^{-1} falloff at high wavenumbers. For these models the transition from sub- to supershear speeds is more complicated than that occurring in models of Fig. 2a; in this case, depending on the fluctuations of the heterogeneous initial stress field, there is a complex mixture of patches of the fault experiencing $v_r > v_S$ and other, larger patches where the opposite holds. The spatial distributions of the rupture velocity resulting from these two synthetic earthquakes are reported in Fig. 10c and d of Bizzarri (2010c) for the RD and SW laws, respectively. Notably, we can see from Fig. 3 that also in this case v_{peak} goes like v_r^2 for rupture velocities up to v_S. Then v_{peak} diminishes and it starts to increase again, roughly in a quadratic manner, as previously observed for homogeneous models (see Fig. 2a). We note that the drop in v_{peak} for the RD case is less evident, since this simulation has small supershear patches, so that $<v_{peak}>$ remains below v_S (see Fig. 4a).

The behavior around v_S is interesting; the significant reduction of peak slip velocities corresponding to the transition from sub- to supershear regime is connected to the loss of high frequencies at

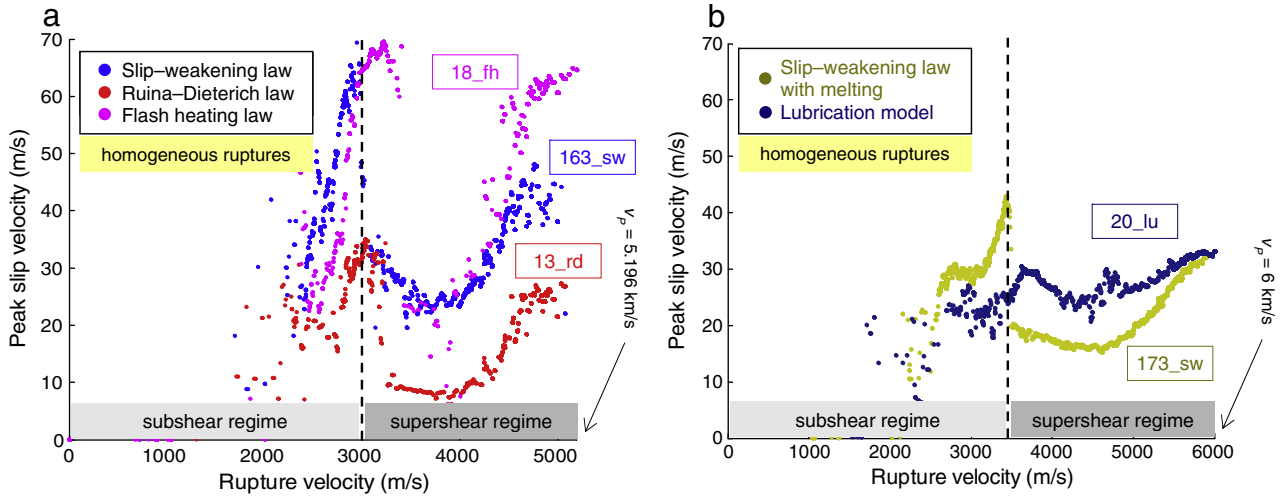

Fig. 2. Results for supershear ruptures (in this case, for the RD law $a = 0.010$ and $b = 0.022$). Results for a case with melting is reported in panel (b); parameters are the same as in Bizzarri (2011a; his Fig. 6, yellow line).

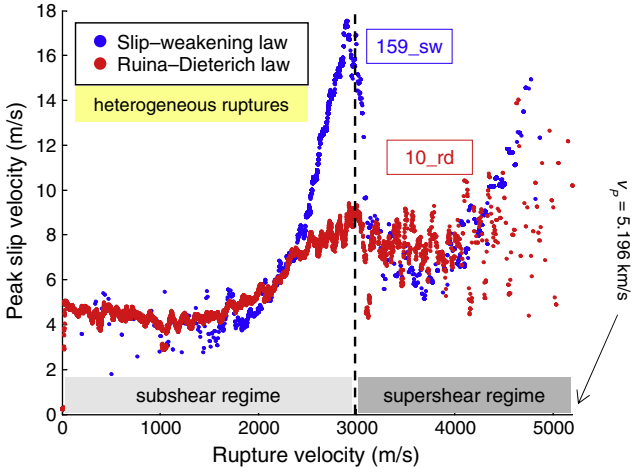

Fig. 3. Heterogeneous simulations; the initial stress distribution is reported in Fig. 10a of Bizzarri (2010c), while the other parameters are the same as in Fig. 1.

the crack tip in supershear ruptures. Moreover, we can also see that the patches of the fault experiencing supershear rupture propagation exhibit values of v_{peak} that are in general smaller than those pertaining to subshear regions, in agreement with previous findings (Bizzarri and Spudich, 2008; Schmedes et al., 2010b). This issue is also discussed in more details in Appendix A.

By looking at Figs. 2 and 3 we can note that there is no a clear evidence of a forbidden region of rupture speeds between the Rayleigh velocity (v_R) and the v_S. Indeed, energetic arguments demonstrated that for purely 2-D, steady-state, non spontaneous cracks the above mentioned range of rupture speeds is inadmissible (Broberg, 1989, 1994, 1999). In the case of 3-D spontaneous ruptures, as those considered here, the coupling of mode II and mode III can allow the rupture speed to extend above v_R slightly, as occurs in the well known elliptical crack solution with mode II velocity of v_R and mode III velocity of v_S (Richards, 1973). Moreover, when the rupture front is not smooth (i.e., it has a kink, due for instance to stress heterogeneities) the nature of the crack tip is markedly different from a 2-D rupture; for this reason is not surprising that Fig. 3 does not exhibits a forbidden range of v_r. We also mention that the difference between v_R and v_S is so small that it is difficult to resolve the rupture velocity with sufficient accuracy to see a forbidden range of rupture speeds. From an observational point of view, it should be also noted that the resolution that is possible to obtain today from recorded seismograms cannot exclude that real-world earthquakes actually pass through these speed regimes while going from sub-Rayleigh to supershear or compressional wave speeds (Das, 2010).

To analyze the data we have adopted a zero-offset spatial correlation analysis, in that we have considered the values of v_{peak} and v_r attained in the same fault node. We will discuss in Appendix B the effects of a nonzero-offset correlation analysis method (Song et al., 2009), where these quantities are compared in different points of the rupture plane (i.e., we introduce some spatial offset).

4. Event by event statistics

In the present section we consider the whole ensemble of the performed numerical experiments and we compute the spatial averages for each event. In particular, we spatially average the values v_{peak} and v_r over the fault nodes experiencing the rupture (namely, for points where the fault slip velocity exceeds the threshold value $v_l = 0.01$ m/s). We also exclude points within the initialization patch, where possible effects of the imposed nucleation can affect the data. Since we consider 3-D ruptures, which is a mixture of inplane (mode II) and antiplane (mode III) modes of propagation are coupled, when we compute the spatial average of v_r we consider both the faults nodes when eventually the rupture speed is supershear (portions of the rupture front experiencing predominantly mode II conditions) and those when it remains subshear.

Our catalog is composed of 76 simulated earthquakes, which cover a range of magnitudes roughly between 5.5 and 7.0 (namely, they span a range of seismic moment between 1.06×10^{17} Nm and 3.66×10^{19} Nm). Overall, our statistics are based upon the analysis of about 200 million fault nodes. This kind of analysis does not consider the details of each individual rupture, such as the transition between the sub- to the supershear regime, local effects of the heterogeneous fault patches, etc., which, on the contrary, are considered in the analysis of each individual event, as that presented in the previous figures. Here, we consider the average behavior of all the synthetic earthquakes.

Fig. 4a confirms that also the averaged v_{peak} and v_r positively correlate. In particular, we can see that $<v_{peak}>$ increases more than linearly with $<v_r>$; we can extrapolate the following relation

$$\left\langle v_{peak}\right\rangle = Ae^{B\frac{\langle v_r\rangle}{v_S}} \tag{2}$$

where $A = 0.67$ m/s, $B = 2.89$. To make our statistic more robust we have also considered some SW cases where the fault is 110 km long and has a high aspect ration ($L^f/W^f = 11$, instead of 0.52 as in the reference simulations). These numerical experiments are denoted by light blue symbols in Fig. 4a and comes from Bizzarri et al. (2010) (as such they have been obtained with a different numerical code). In these cases the rupture accelerates and finally propagates at nearly constant speeds when the fault properties are homogeneous (see Fig. 2 of Bizzarri et al., 2010), in agreement with the findings of Schmedes et al. (2010b). At the same time, we also have that v_{peak} tends to saturate (see Animations S1 and S2 of the auxiliary material of Bizzarri et al., 2010) at moderate to large distance from the hypocenter, when the rupture has fully developed. By considering these saturations values in the averaging procedure we still obtain a god agreement with the prediction of the empirical relation (2), as shown in Fig. 4a.

The maximum variations of v_{peak} are expected to take place during the accelerating stage of the rupture (where v_r changes significantly, too). In this phase it has been found for 2-D SW ruptures that the cohesive zone (where the stress is released) progressively shrinks (Andrews, 1976). In homogeneous conditions this implies that, when the rupture is accelerating, also the peak slip velocity increases as the rupture develops (Bizzarri et al., 2001; their Equation (A5)).

Moreover, our results indicate that the average v_{peak} increases with the magnitude of the event (see Fig. 4b). If we exclude the FH simulations (symbols in magenta in Fig. 4a) – which are known to give an overestimate of the fault slip velocities (Bizzarri, 2009; Noda et al., 2009) – although there is considerable scatter, we can tentatively fit the data with a curve of the type $<v_{peak}> \sim M_0^{0.18}$.

5. Discussion and concluding remarks

In addition to the fracture energy density, the stress drop, and the total developed slip, very important dynamic variables which characterize the earthquake source physics are the rupture speed (v_r) and the peaks in fault slip velocity (v_{peak}). While the fault slip velocity is related to the ground motions (Aki and Richards, 2002), the rupture speed is known to affect the high frequency signature of the ground velocity time histories (Bizzarri et al., 2010). Moreover, a pivotal question in seismic hazard assessment is to clarify how the peak ground velocity scales with the earthquake magnitude (Abrahamson and Silva, 2008).

Hitherto, a systematic analysis of the spatial correlation existing between v_{peak} and v_r for different constitutive models and stress conditions was lacking. The present work fill this gap, through the analysis of a synthetic catalog composed by 76 earthquakes which cover a

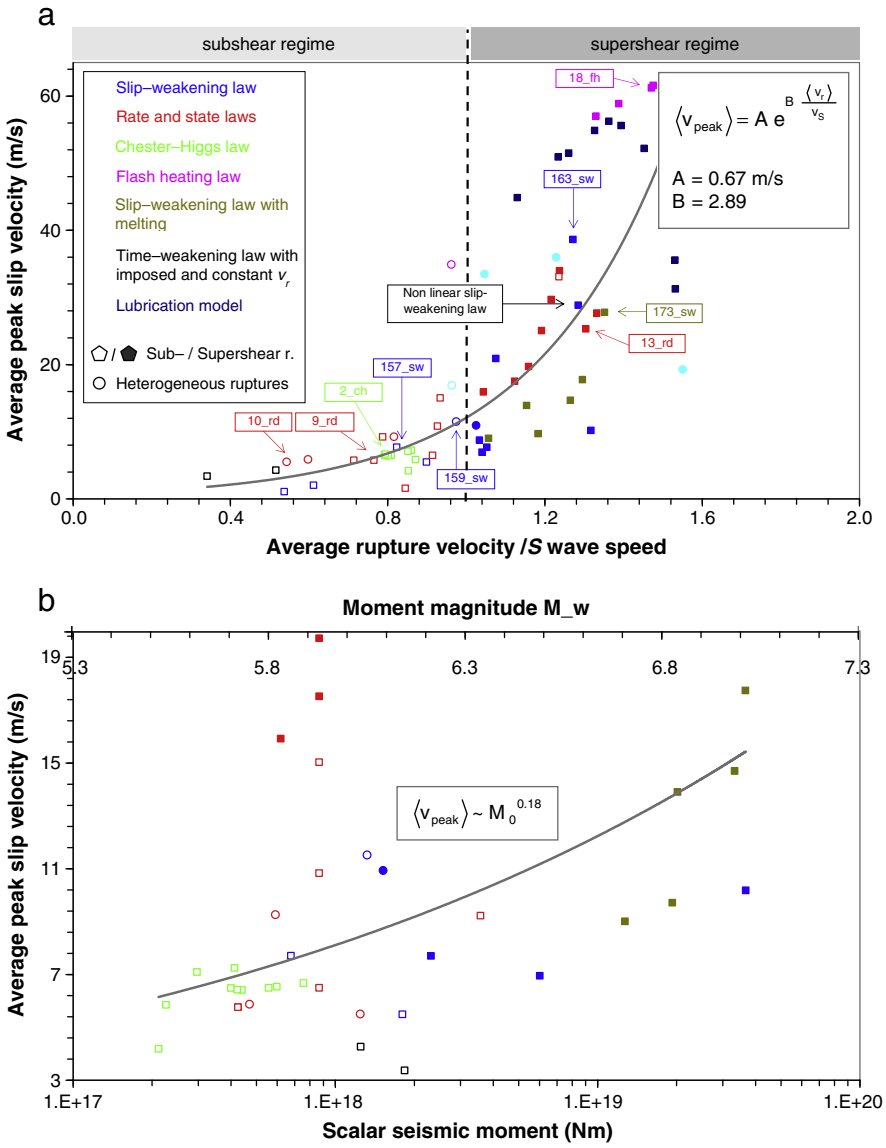

Fig. 4. Results for the event by event statistics where we spatially average the values of v_{peak} and v_r for all the considered synthetic earthquake of our catalog. Blue indicates SW law (light blue identifies SW simulations with the elastic parameters and fault dimension as in Bizzarri et al., 2010). We also include a model with a non-linear SW law (see Bizzarri, 2010a; his Fig. 4). Red denotes the RS laws (in addition to the Ruina–Dieterich law we also consider the Dieterich–Ruina ageing model), green indicates CH law, magenta indicates FH law and brown indicates SW law with melting effects. Finally, black identifies the simulations with a prior-imposed and constant rupture speed. All the equations are summarized in Table 1. Open and full and symbols refer to sub- and supershear ruptures, respectively. Circles represent heterogeneous configurations. (a) Average v_{peak} as a function of the average v_r. Labels emphasize the numerical experiments presented in the previous three figures. (b) Average v_{peak} as a function of the size of the event. M_0 and M_w refer to the whole fault length on which the bilateral ruptures develop.

wide magnitude interval (M_0 from 1.06×10^{17} Nm to 3.66×10^{19} Nm) and propagate spontaneously on planar faults, obeying a large number of governing models.

One conclusion emerging from our study is that v_{peak} and v_r correlate for all the governing equations we consider, confirming the results obtained with the linear slip-weakening law (Schmedes et al., 2010a). In particular, we found here that the peak fault slip velocity increases as the rupture speed increases. Interestingly, the direct dependence between v_{peak} and v_r is more than linear, as previously suggested by laboratory fracture experiments performed at relatively low velocities and for the purely in-plane geometry (Ohnaka et al., 1987; see Eq. (1)). Indeed, the event by event statistics over all the 3-D spontaneous rupture models we consider indicate that peak slip velocity averaged over the fault surface increases exponentially with the average rupture speed (Fig. 4a), as stated by Eq. (2). This conclusion is robust, in that it holds for both sub- and supershear ruptures, both in homogeneous and heterogeneous conditions. Moreover, this result is confirmed for a large class of constitutive equations, conceptually different and based upon different physical frameworks (Bizzarri, 2011b); the linear slip-weakening, the classical (or canonical) formulations of the rate and state laws with memory effects, the flash heating of micro-asperity contacts model and the Chester and Higgs model (a compendious summary of the equations is reported in Table 1). This result is important, in that we can extract consistent correlation patters irrespective of the assumed friction law.

Our numerical experiments also suggest a direct dependence of $<v_{peak}>$ on M_0; this is reported in Fig. 4b, which indicates that the average peak slip velocity roughly goes like $M_0^{0.18}$. This relation holds by excluding FH simulations which predict very high values, perhaps overestimates, of the fault slip velocity, as previously noted (Bizzarri, 2009; Noda et al., 2009). In other words, we found that the more destructive the earthquake is, the more relevant peaks in

fault slip velocity are attained. This has also consequences on the heat dissipated during sliding, which is directly controlled by the values of the slip velocity (Richards, 1976).

Several empirical studies (Abrahamson and Silva, 2008; Boore and Atkinson, 2008) suggest that peak ground velocity (PGV) increases with the magnitude of the event and saturates for moments greater than roughly 4×10^{19} Nm. It is difficult to relate the peak fault slip velocity to PGV; if the peaks on the fault occur during a very short duration, they might be destroyed by anelastic attenuation during the propagation in the medium surrounding the fault surface, or they might not add constructively at a receiver site. On the other hand, the longer period components would survive and add constructively to make the PGV. Finally, we note that if peak slip velocities are largest away from the hypocenter, then they occur in an area where the isochrones velocities are smaller (see Schmedes and Archuleta, 2008), countering the effect of large v_{peak}.

Moreover, we found that significant peaks in slip velocity can be realized (see Fig. 4); there is a large debate in the literature concerning the existence of extreme ground motions (Harris et al., 2011).

We conclude by emphasizing that the spatial interdependencies between the dynamic variables we found can be implemented as constraints in kinematic modeling of faults. A further development of this work is to explore whether the above conclusions are also preserved for more complex geometries, which account for fault bending and non planarity of the fault surfaces.

Acknowledgments

Discussion with P. Spudich improved the manuscript. I wish to thanks the Editor, L. P. Stixrude, S. G. Song and one anonymous referee for some interesting comments and useful suggestions. F. Pintori is acknowledged for assisting in the preparation of some figures.

Appendix A. Distribution of the peak slip velocity on the fault surface

In Fig. A1 we report the spatial distribution over the fault plane of the peak slip velocity (v_{peak}) for homogeneous supershear ruptures. Panel (a) refers to a slip-weakening case (which corresponds to the blue circles in Fig. 2a of the main text), while panel (b) refers to a Ruina–Dieterich model (which corresponds to the red circles in Fig. 2a of the main text). Due to the symmetry exploitation (see Bizzarri, 2009 for the numerical details) we plot only one half of the fault in the strike direction.

In both the panels we also superimpose the contours defining the transition between the sub- and the supershear regimes, where the local rupture speed (v_r) is below and above the S wave speed (v_S), respectively.

It is apparent from Fig. A1 that the fault patches where the rupture remains subshear (which are in the direction of the mode III propagation, i.e., perpendicular with respect to the direction of the initial stress, aligned along the strike direction) exhibit higher peaks in fault slip velocity, on average, with respect to the supershear regions (which are in the direction of the mode II propagation, i.e., on the strike direction). This is in agreement with the findings of Bizzarri and Spudich (2008).

The fact that v_{peak} tends to be higher in the mode III (i.e., antiplane) direction than in the mode II (i.e., inplane) direction is a feature which is preserved also for subshear rupture events; this is evident from Fig. A2, where we plot the spatial distribution of v_{peak} for the Ruina–Dieterich model (panel (a)) and for the Chester–

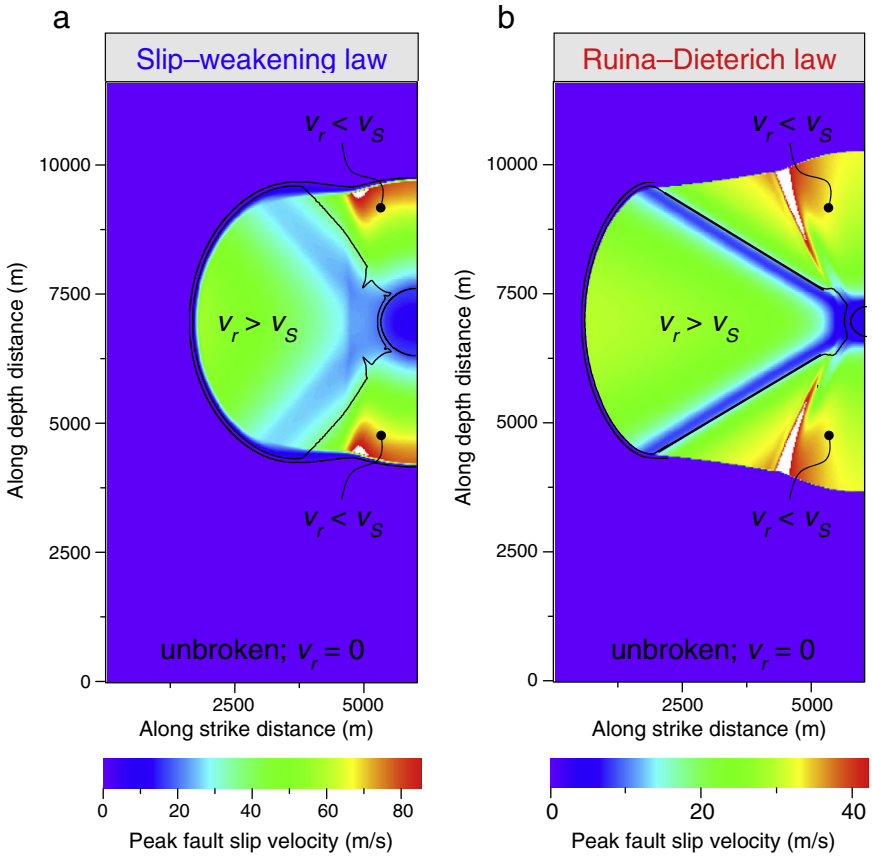

Fig. A1. Spatial distribution of the peak fault slip velocity for the slip-weakening law (panel (a)) and for the Ruina–Dieterich model (panel (b)). The two configurations correspond to blue and red circles of Fig. 2a of the main text, respectively. In both panels purple regions identify the unfractured parts of the fault. Patches experiencing the sub- and supershear rupture propagation are also indicated. Since the rupture is bilateral we plot only one half of the fault length.

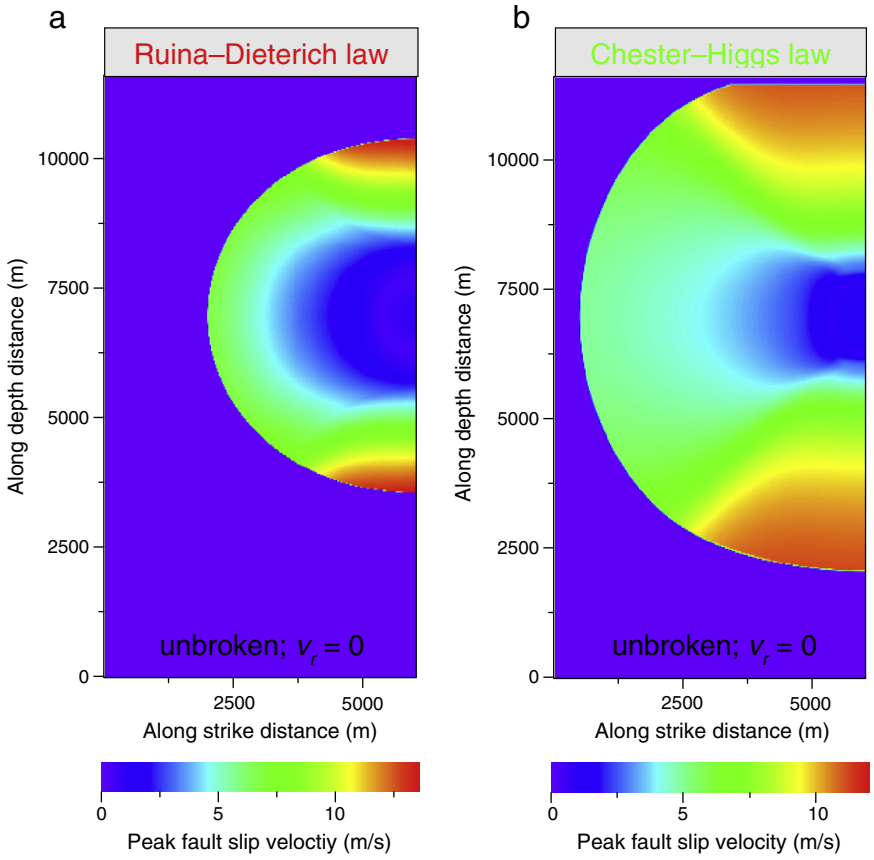

Fig. A2. The same as in Fig. A1, but now for two subshear ruptures; panel (a) corresponds to red circles of Fig. 1 of the main text, while panel (b) corresponds to green circles in that figure.

Higgs model (panel (b)), presented in Fig. 1 of the main text (red and green circles, respectively). This is the reason why it is a common practice to examine the fault slip velocity time histories in the anti-plane direction when the modeler wants to analyze the quality of its solutions, in term of numerical oscillations.

Appendix B. The nonzero-offset correlation analysis method

In the grid by grid analysis presented in Section 3 we have considered a zero-offset distance correlation analysis (i.e., we have considered the values of the peak fault slip velocity and of the rupture speed in the same fault node). We will consider here a nonzero-offset distance correlation, in which these quantities are defined in different points of the fault plane.

To this goal we follow the approach discussed in Bizzarri (2010c); in particular, we consider the normalized covariance as it follows (e.g., Goovaerts, 1997):

$$C_{\alpha,\beta} = \frac{\sum_{i=1}^{i_{end}-\alpha+1} \sum_{k=1}^{k_{end}-\beta+1} \left(x_{i,k}-\langle X\rangle\right)\left(y_{i+\alpha-1,k+\beta-1}-\langle Y\rangle\right)}{(i_{end}-\alpha+1)\,(k_{end}-\beta+1)\,\sigma_X\sigma_Y} \tag{B.1}$$

where the 2-D arrays X and Y denote the arrays v_{peak} and v_r, respectively, and $\langle X\rangle = \frac{1}{i_{end}k_{end}} \sum_{i=1}^{i_{end}} \sum_{k=1}^{k_{end}} x_{i,k}$ and $\sigma_X = \sqrt{\frac{1}{i_{end}k_{end}} \sum_{i=1}^{i_{end}} \sum_{k=1}^{k_{end}} \left(x_{i,k}-\langle X\rangle\right)^2}$ (and analogous expressions for Y). In Eq. (B.1) the operator $\langle\cdot\rangle$ represents the average value of the array and σ its standard deviation. The integers i_{end} and k_{end} define the size of the arrays in the x_1 (strike) and x_3 (depth) directions, respectively, while the integers α and β define the translation vector $\mathbf{h} \equiv ((\alpha-1)\Delta x_1,\ (\beta-1)\Delta x_3) = ((\alpha-1),(\beta-1))\Delta x$ (Δx being the spatial discretization; see Table 2) $\mathbf{h}$ is associated to the spatial offset distance $h = \sqrt{(\alpha-1)^2+(\beta-1)^2}\Delta x$ and an azimuth angle $\varphi = \mathrm{arctg}(\beta-1)/(\alpha-1))$.

The pair $(\alpha,\beta) = (1,1)$ corresponds of a zero–offset distance, so that $C_{\alpha,\beta}$ becomes the autocorrelation function. $C_{\alpha,\beta}$, which is also known as correlogram (Goovaerts, 1997), represents the linear dependency between the two variables X and Y, and it varies between -1 and 1 (see also Song et al., 2009). The evaluation of $C_{\alpha,\beta}$ for different values of h (i.e., for different values of α and β) quantifies the potential spatial coherence between the spatially varying variables X and Y.

We have considered two rather different datasets, one pertaining to a SW law leading to a supershear rupture and one pertaining to a RS simulation where the rupture remains subshear. The results are reported in Fig. B1a and b, respectively, where we report the values of $C_{\alpha,\beta}$ as a function of the spatial offset h. It is clear that the maximum spatial correlation exists at zero–offset distance for both the models. Remarkably, this feature is not peculiar of these numerical simulations, but it emerges for the whole ensemble of models we have considered. We can also see from Fig. B1 that for increasing spatial offset $C_{\alpha,\beta}$ decreases, reaching a minimum for a value of h value nearly equal to 2.3 km for both the models, while the slopes of the three curves reported in Fig. B1a and b is slightly different.

We can conclude that the maximum spatial correlation existing at zero–offset distance corroborates the same point, grid by grid analysis presented in Section 3.

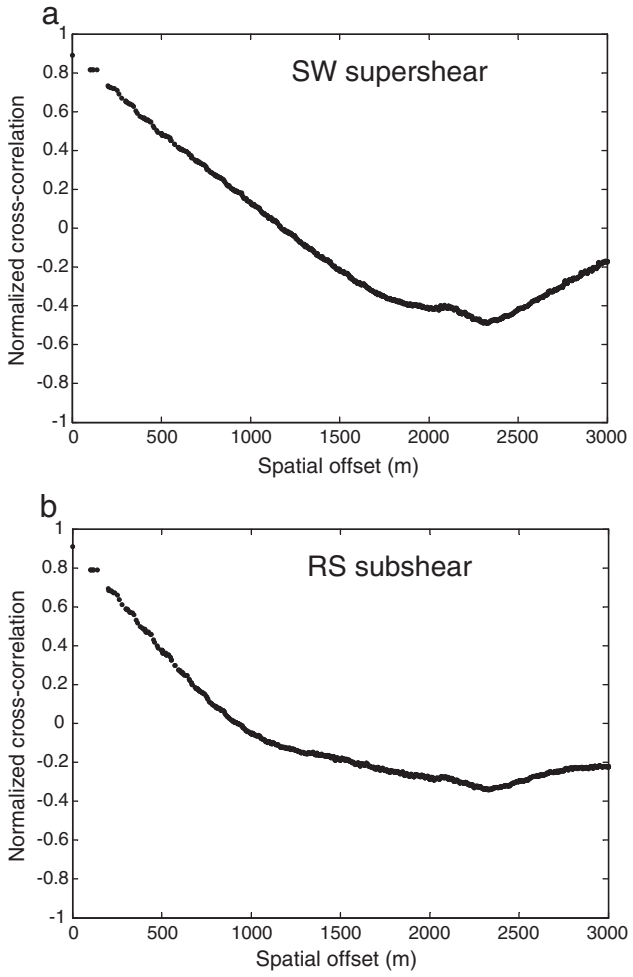

Fig. B1. Results for the non-zero offset correlation analysis method. For two different models, a supershear rupture obeying the SW law (panel (a)) and a subshear rupture governed by RS law (panel (b)), we plot the values of the normalized covariance $C_{\alpha,\beta}$ between v_{peak} and v_r as a function of the spatial offset $h=\sqrt{(\alpha-1)^2+(\beta-1)^2}\Delta x$. $C_{\alpha,\beta}$ is formally defined in Eq. (B.1). We can clearly see that the maximum correlation exists at zero offset distance for both the models.

References

Abrahamson, N., Silva, W., 2008. Summary of the Abrahamson & Silva NGA ground motion relations. Earthquake Spectra 24, 67–97.

Aki, K., Richards, P.G., 2002. Quantitative Seismology, 2nd ed. University Science Books, Sausalito, CA, USA. (700 pp.).

Andrews, D.J., 1976. Rupture velocity of plane strain shear cracks. J. Geophys. Res. 81 (32), 5679–5687.

Andrews, D.J., Barral, M., 2011. Specifying initial stress for dynamic heterogeneous earthquake source models. Bull. Seismol. Soc. Am. 101 (No. 5), 2408–2417. doi:10.1785/0120110012.

Bhat, H.S., Dmowska, R., King, G.C.P., Klinger, Y., Rice, J.R., 2007. Off–fault damage patterns due to supershear ruptures with application to the 2001 Mw 8.1 Kokoxili (Kunlun) Tibet earthquake. J. Geophys. Res. 112 (B06301). doi:10.1029/2006JB004425.

Bizzarri, A., 2009. Can flash heating of asperity contacts prevent melting? Geophys. Res. Lett. 36, L11304. doi:10.1029/2009GL037335.

Bizzarri, A., 2010a. An efficient mechanism to avert frictional melts during seismic ruptures. Earth Planet. Sci. Lett. 296, 144–152. doi:10.1016/j.epsl.2010.05.012.

Bizzarri, A., 2010b. Pulse-like dynamic earthquake rupture propagation under rate-, state- and temperature-dependent friction. Geophys. Res. Lett. 37, L18307. doi:10.1029/2010GL044541.

Bizzarri, A., 2010c. On the relations between fracture energy and physical observables in dynamic earthquake models. J. Geophys. Res. 115, B10307. doi:10.1029/2009JB007027.

Bizzarri, A., 2011a. Dynamic seismic ruptures on melting fault zones. J. Geophys. Res. 116, B02310. doi:10.1029/2010JB007724.

Bizzarri, A., 2011b. On the deterministic description of earthquakes. Rev. Geophys. 49, RG3002. doi:10.1029/2011RG000356.

Bizzarri, A., submitted for publication. The mechanics of lubricated faults: Insights from 3-D numerical models, J. Geophys. Res.

Bizzarri, A., Cocco, M., 2005. 3D dynamic simulations of spontaneous rupture propagation governed by different constitutive laws with rake rotation allowed. Ann. Geophys. 48 (2), 279–299.

Bizzarri, A., Spudich, P., 2008. Effects of supershear rupture speed on the high-frequency content of *S* waves investigated using spontaneous dynamic rupture models and isochrone theory. J. Geophys. Res. 113, B05304. doi:10.1029/2007JB005146.

Bizzarri, A., Cocco, M., Andrews, D.J., Boschi, E., 2001. Solving the dynamic rupture problem with different numerical approaches and constitutive laws. Geophys. J. Int. 144, 656–678.

Bizzarri, A., Dunham, E.M., Spudich, P., 2010. Coherence of Mach fronts during heterogeneous supershear earthquake rupture propagation: Simulations and comparison with observations. J. Geophys. Res. 115, B08301. doi:10.1029/2009JB006819.

Boore, D.M., Atkinson, G.M., 2008. Ground motion prediction equations for the average horizontal component of PGA, PGV, and 5%-damped PSA at spectral periods between 0.01 s and 10 s. Earthquake Spectra 24, 99–138.

Broberg, K.B., 1989. The near-tip field at high crack velocities. Int. J. Fract. 39, 1–13.

Broberg, K.B., 1994. Intersonic bilateral slip. Geophys. J. Int. 119, 706–714.

Broberg, K.B., 1999. Cracks and Fracture. Academic Press, New York.

Burridge, R., 1973. Admissible speeds for plane-strain self-similar shear crack with friction but lacking cohesion. Geophys. J. R. Astron. Soc. 35, 439–455.

Chester, F.M., Higgs, N.G., 1992. Multimechanism friction constitutive model for ultrafine gouge at hypocentral conditions. J. Geophys. Res. 97 (No. B2), 1859–1870.

Das, S., 2010. Earthquake supershear rupture speeds. Tectonophysics 493, 213–215. doi:10.1016/j.tecto.2010.07.009.

Freund, L.B., 1979. The mechanics of dynamic shear crack propagation. J. Geophys. Res. 84, 2199–2209.

Goovaerts, P., 1997. Geostatistics for Natural Resources Evaluation, Applied Geostatistics Series. Oxford Univ. Press, New York.

Guatteri, M., Mai, P.M., Beroza, G.C., 2004. A pseudo-dynamic approximation to dynamic rupture models for strong ground motion prediction. Bull. Seismol. Soc. Am. 94 (No. 6), 2051–2063. doi:10.1785/0120040037.

Harris, R.A., et al., 2011. Verifying a computational method for predicting extreme ground motion. Seismol. Res. Lett. 82 (No. 5), 638–644. doi:10.1785/gssrl.82.5.638.

Mikumo, T., Olsen, K.B., Fukuyama, E., Yagi, Y., 2003. Stress–breakdown time and slip-weakening distance inferred from slip–velocity functions on earthquake faults. Bull. Seismol. Soc. Am. 93, 264–282.

Noda, H., Dunham, E.M., Rice, J.R., 2009. Earthquake ruptures with thermal weakening and the operation of major faults at low overall stress levels. J. Geophys. Res. 114, B07302. doi:10.1029/2008JB006143.

Ohnaka, M., Kuwahara, Y., Yamamoto, K., 1987. Constitutive relations between dynamic physical parameters near a tip of the propagating slip zone during stick–slip shear failure. Tectonophysics 144, 109–125.

Richards, P.G., 1973. The dynamic field of a growing plane elliptical shear crack. Int. J. Solids Struct. 9, 843–861.

Richards, P.G., 1976. Dynamic motions near an earthquake fault: a three dimensional solution. Bull. Seismol. Soc. Am. 66, 1–32.

Schmedes, J., Archuleta, R.J., 2008. Near–source ground motion along strike–slip faults: insights into magnitude saturation of PGV and PGA. Bull. Seismol. Soc. Am. 68 (5), 2278–2290.

Schmedes, J., Archuleta, R.J., Lavallée, D., 2010a. Correlation of earthquake source parameters inferred from dynamic rupture simulations. J. Geophys. Res. 115, B03304. doi:10.1029/2009JB006689.

Schmedes, J., Archuleta, R.J., Lavallée, D., 2010b. Dependency of supershear transition and ground motion on the autocorrelation of initial stress. Tectonophysics 493, 222–235. doi:10.1016/j.tecto.2010.05.013.

Song, S.G., Sommerville, P., 2010. Physics-based earthquake source characterization and modeling with geostatistics. Bull. Seismol. Soc. Am. 100 (No. 2), 482–496. doi:10.1785/0120090134.

Song, S.G., Pitarka, A., Sommerville, P., 2009. Exploring spatial coherence between earthquake source parameters. Bull. Seismol. Soc. Am. 99, 2564–2571. doi:10.1785/0120080197.

Tinti, E., Bizzarri, A., Piatanesi, A., Cocco, M., 2004. Estimates of slip weakening distance for different dynamic rupture models. Geophys. Res. Lett. 31, L02611. doi:10.1029/2003GL018811.